Bulletin of Environment, Pharmacology and Life Sciences
Bull. Env. Pharmacol. Life Sci., Vol 13 [7] June 2024: 115-124

Online ISSN 2277-1808
Journal's URL: http://www.bepls.com
CODEN: BEPLAD

ORIGINAL ARTICLE **OPEN ACCESS**

Investigation of Structural Characterization and Biological applications of supported MoO_3/SiO_2 nanocomposite

Prashant Shinde,[1] Mukund Ambawade[2], Shobha Waghmode[3] and Sharda Gadale[*1]
[1] Dept. of chemistry, Yashwantrao Mohite College of Arts Science and Commerce,
Bharati Vidyapeeth (Deemed To Be University), Pune, India
[2]Haribhai V. Desai College, Pune
[3]Garware College, Pune
***Corresponding Address**: Sharda Gadale
Email: dagade@rediffmail.com

ABSTRACT
In the present paper we have discussed Fe supported on MoO_3/SiO_2 (FMS) catalyst system for the biological applications by means of Antibacterial activity of the test material was performed by Agar Well Diffusion Method. FMS catalysts prepared by using sol-gel synthesis method and well characterized by spectroscopic and microscopic methods such as X-ray diffraction (XRD), Scanning Electron microscope (SEM), Energy Dispersive Spectrometer (EDX), Ultra Violet (UV) spectroscopy, Fourier transform Infra-Red (FT-IR). The crystallite size of the synthesized samples was calculated by Scherer's equation using XRD analysis. All the FMS samples (1FMS, 5FMS, 10FMS, 15FMS & 20FMS) showed good antibacterial activity against Escherichia coli, Klebsiella pneumonia, Pseudomonas aeruginosa, Bacillus subtilis, Staphylococcus aureus, Candida albicans and Aspergillus niger. The FMS catalysts significantly reduce formation of Staphylococcus aureus, Pseudomonas aeruginosa and E. coli biofilm as the concentration of FMS increases.
Keywords: *Supported catalyst, Nanomaterial, XRD, Antimicrobial, Antibiofilm activity*

Received 19.04.2024 Revised 29.05.2024 Accepted 25.06.2024

INTRODUCTION

Human lives are significantly impacted by environmental pollution carried on by growing urbanisation and industrialisation. In the various such chemical, plastic ..etc industries where these noxious organic dyes are the byproducts of industrial processes, a large amount of non-biodegradable as well as cancer-causing coloured dyes are regularly discharged in freshwater systems[1],[5] Hazardous contaminants present in industrial wastewater include heavy metal ions, inorganic compounds including mineral acids, trace elements, inorganic salts, sulphates, and metal complexes, as well as organic constituents such pesticides, polyaromatic hydrocarbons, dyes, and phenols [6]. Different types of dyes used in industries are found in wastewater. Due to their potential toxicity and carcinogenicity, dyes like methylene blue (MB), phenothiazine, methylene orange, rhodamine B, and triphenylmethane represent a significant environmental hazard to living humans [7]. MB is a cationic (positively charged) organic dye that is widely used in a variety of sectors, including the textile, veterinary, and pharmaceutical industries [8]. However, it has been linked to several health problems and water contamination. MB has a number of harmful impacts on human health, including problems with nausea, vomiting, respiration, and gastritis. So, to maintain life on Earth, water must be purified, which is a huge research barrier. In this context, numerous methods for purifying water have emerged, including desalination, reverse osmosis for the degradation of dyes, ultrafiltration, co-precipitation, catalysis, and photocatalysis activities [9]. Industries discharge environmental waste, which must be transformed into a useful form before being disposed of in freshwater resources. Waste recovery strategies have been used to treat water in an economical and sustainable manner [10]. The use of manmade wetlands for sewage treatment is commonplace worldwide. To assess the long-term efficacy of the domestic sewage treatment wetland system, groundwater and surface water contamination may happen [11]. The most popular methods for eliminating contaminants from industrial wastewater are ion exchange, photocatalysis, electrolysis, carbon filtering, reverse osmosis, microbial control adsorption, and nanofiltration [12,13]. Among the discussed methods, the most desirable method is catalysis since it is economical, environmentally friendly, and energy-efficient [14].

In the dairy sector, Mastitis is one of the most prevalent diseases which causes financial harm and a decrease in milk output globally. Mastitis is linked to pathological changes in the mammary gland system and physical changes in the chemistry of milk. Mastitis is one of several illnesses brought on by microorganisms, which include fungus, viruses, and bacteria [15]. *E. coli* and *S. aureus*. *S. aureus* is the most common multi drug resistant bacteria which causes nosocomial contagions in hospitals and other healthcare facilities. Numerous drug-resistant bacteria, including Gram-positive (*S. aureus*) and Gram-negative (*E. coli*) bacteria, have generated novel species in recent years, presenting a significant health risk to humans [16]. Large amounts of metal oxides (MOs) have been utilised to eliminate pathogenic harmful bacteria and degrade organic pollutants in industrial wastewater. Nanosized metallic oxides are used in a wide range of technological and industrial applications, some of which include optical, mechanical, and environmental and optical components [17]. It has been considered that transition and rare metal oxides, such as CeO2, MnO2, TiO2, SnO2, Fe3O4, MoO3, and CaO2, are promising for disinfection, hydrogen generation, and water purification [18]. Among these, Fe3O4 is one of the most prevalent n-type semiconductor materials with a narrow band gap and high surface area, and it has significant optoelectrical and chemical applications because of its many characteristics, including effectiveness and economy, environmental friendliness, inertness to chemical changes, and excellent biocompatibility [19]. In addition to restricting the use of MOs in photocatalytic applications, the combination of metal and MOs enhances the recombination of photogenerated electrons and holes [21]. As an electron mediator, Mo-Fe2O3 serves to capture generated electrons and aid in the effective application of electron conductivity. The purpose of this study was to evaluate the effectiveness of a sol-gel-synthesised Fe/Mo/SiO2 catalyst for dye degradation and antimicrobial performance. The produced samples were then employed to remove contaminants from wastewater through catalytic reduction. Moreover, the optical, morphological, and structural properties of Fe_3O_4 and Mo-doped Fe_3O_4 were analyzed using X-ray diffractometry (XRD), Fourier transform infrared (FTIR) spectroscopy, scanning electron microscopy (SEM), energy-dispersive X-ray spectroscopy (EDS), mapping, ultraviolet-visible (UV-vis) and anti-microbial experiments against Gram-negative, Gram positive bacterial and fungal species. Since long Silver nanoparticles (AgNPs) have been proposed as efficient agents to fight the increasing number of antibiotic-resistant pathogens as well as good antibiofilm agent [28]. The Betulinan C and its analogs was found good biofilm inhibitory activity against *Pseudomonas aeruginosa O1*[29]. This study points towards an alternative for the treatment of microbial infections and biofilm-induction, with the probability of decreasing the threat of multidrug resistance.

MATERIAL AND METHODS

Materials

All the reagent viz., tetraethyl orthosilicate (TEOS), ammonium molybdate (AHM), Ferric nitrate, isopropyl alcohol, methyl orange and bromothymol blue were of A.R grade and were obtained from Merck chemicals, India.

Media: Nutrient Agar for Bacterial cultures and Yeast Extract Peptone Glucose Agar/ Potato dextrose agar for fungal cultures

Bacterial cultures: *Escherichia coli, Klebsiella pneumonia, Pseudomonas aeruginosa, Bacillus subtilis, Staphylococcus aureus, Candida albicans* and *Aspergillus niger*

Method

To compare the catalytic activity of synthesized catalyst, catalysts prepared by sol-gel method and characterized by various spectroscopic methods including X-ray diffraction (XRD), Scanning Electron microscope (SEM), Energy Dispersive Spectrometer (EDX), Ultra Violet (UV) spectroscopy, flourier transfer Infra-Red (FT-IR) spectroscopy. The crystallite size of the synthesized samples was calculated by XRD using Rigaku Miniflex G-500 diffractometer equipped with a Ni filtered Cu-Kα line radiation source (λ=1.54178 Å) was used to record. Scanning Electron Microscope coupled with EDX (JEOL-JSM 6360A) was used for external surface of hybrid material. SEM and Energy dispersive X-ray analysis detector (EDX) were obtained at accelerating voltage 20 KeV. FT-IR and UV were carried out by using Shimadzu instrumentations.

Synthesis of $Fe/Mo/SiO_2$ by Sol-gel method:

Iron supported on MoO_3/SiO_2 (FMS) were synthesized with varying wt. % of Fe oxide concentration (1, 5, 10, 15, and 20 wt.%) in a typical procedure. 10 wt. % FMS was synthesized by dissolving calculated amount of AHM in 40 ml distilled water in sonicator for 60 min. This solution was added drop wise to the tetra ethyl orthosilicate (40 g) under stirring. Then, to this mixture, aqueous solution of calculated amount of ferric nitrate was added and transparent gel was obtained, further material was air dried and then heated in oven at 100 ºC for 12 hr., calcined at 500 ºC for 5 hrs. Similarly, other nano materials were prepared with 1, 5,10, 15, and 20 wt. % FMS.

Photocatalytic activity studies

The effect of the presence of the catalyst on the photodegradation of MB dye was evaluated under visible light irradiation. The solution of 10 mg of dye powder in 100 ml distilled water was prepared. About 0.2 gm of FMS catalysts was added to 100 ml of dye solution. To develop equilibrium between the catalyst and substrate, the suspension was stirred for 30 min in dark prior exposing to visible light. After that the suspension was irradiated with visible light at constant stirring. 3mL of the suspension was taken regularly from the reactor at different irradiation time intervals. The catalytic performance of the catalyst was analyzed quantitatively for the absorption peak at 470 nm of MB in aqueous heterogeneous solution suspensions. The following formula was used to calculate the percentage of dye degradation.

Degradation Efficiency ={(C0-Ct)/C0}×100 …………….. (1)

Where C0 is the initial concentration of the dye solution, Ct is the concentration of the dye solution after photo irradiation in a selected time interval. The growth of biofilm was quantitatively determined according to the "Protocols to study the physiology of oral biofilms" [27].

Statistical analysis: In this investigation, for morphological responses, experiment repeated in three times and results were expressed as Mean±SD.

RESULT AND DISCUSSION:

XRD analysis:

Measurement of the samples was carried out for understanding the structural property as well as other information related to the particle size of the prepared nanocatalyst of various amount of (1, 5, 10,15 and 20 wt. %) Fe doped on MoO_3/SiO_2 were investigated by Xray diffraction studies over the 2θ values in the range of 10-80°.The powdered samples calcined at 500°C (5 h) showed slight crystalline nature. The crystalline nature of iron oxide doped nanoparticles were identified and confirmed from powder X-ray diffraction (XRD) analysis. The diffraction peak for α-MoO_3 can be assigned to 12.94°, 25.79°, 27.80°, 34.08°, 35.97° and 49.72° indexed as (020), (040), (021), (111), (041) and (002). Which exactly matches with (JCPDS NO-01-073-6497) and (JCPDS NO-00-25-1434), The XRD data of iron oxide magnetic nanoparticles are in agreement with the standard value of Fe3O4 (JCPDS file no: 65- 3107). XRD analysis of the particles (Figure 2) shows well defined Bragg reflection characteristics of Fe3O4. The data shows diffraction peaks at 2 θ = 30.05°, 35.451°, 53.516°, 56.998, and 74.01°, which can be indexed to the (220), (311), (422), (511) and (533) planes of Fe3O4 in a cubic phase, respectively [22].

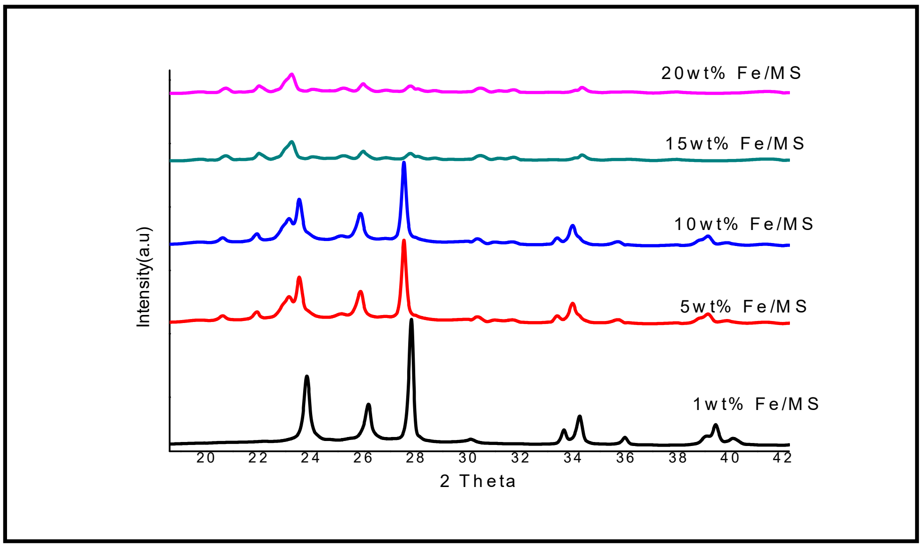

Figure:1. XRD graph of 1-20wt% Fe/MS

The Scherrer equation was applied to estimate the average crystallite sizes of Fe/MS samples: D=$K\theta$, where B is the half-height width of the diffraction peak of anatase, K=0.89 is a coefficient, θ is the diffraction angle, λ is the X-ray wavelength corresponding to the Cu Kα irradiation (1.5406 Å), and D is the average crystallite size of the powder sample.

FTIR Studies:

The successful modifications of the nanoparticles surface were confirmed by Fourier transform infrared spectroscopy (FTIR). FT-IR and UV were carried out by using Shimadzu instrumentations between 4000 and 500 cm-1 The FTIR absorption spectra of 1-20wt% Fe/MS are shown in figures 2. In the spectra of Fe/MS samples showed intensive bands at around 1070.3cm^{-1},1096.33cm^{-1},806.10cm^{-1} are ascribed to Si-

O vibration of SiO_2 and peaks at around 970 cm^{-1}, 995 cm^{-1}, 1320 cm^{-1}, 1500 cm^{-1} corresponding to α-MoO_3 stretching mode these bands confirmed the successful linkage of the molybdenum oxide (MoO_3) with the silica. A weak absorption band appeared at around 1615.18 cm^{-1}due to flexural vibration of the O-H bond absorbed water and hydroxyl on the sample surface contribute to these absorption bands. [23,24]. The presence of absorption peaks in the region of wave numbers 550-630 cm-1 corresponding to the Fe-O vibration.

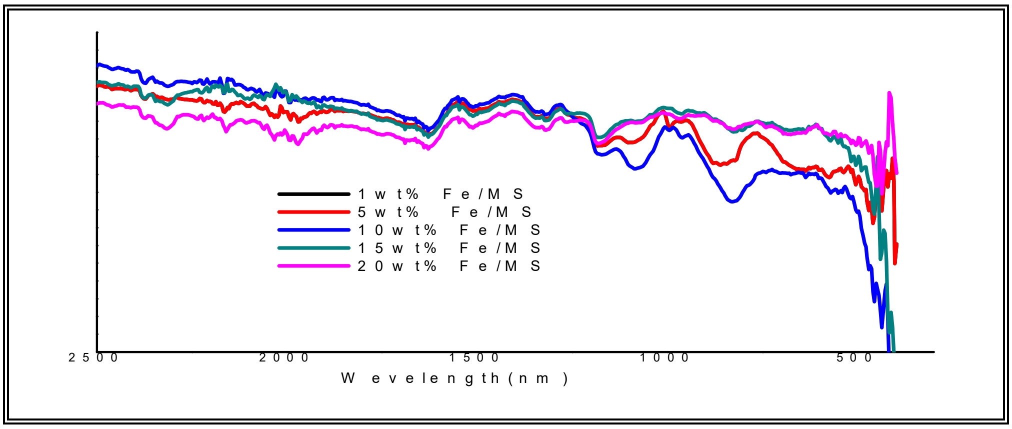

Figure:2. FT-IR graph of 1-20wt% Fe/MS.

FE-SEM Analysis :

The morphological study of prepared Fe/MS nanostructures was carried out using FESEM technique calcined at 5000C temperature images represented in Figure 3(a). It clearly showed that, the Fe loading over MS catalysts were aggregated and agglomerated each other on the catalyst surface to form rough surface morphology. However, it can be seen that the catalyst having smaller particle size with many pores formed which plays an important role to exhibit the higher catalytic activity. All SEM micrographs indicated that, the prepared catalysts have spherical shape of particles [25] as shown in fig. Therefore Sol-Gel method was more efficient to form the uniform structure of the prepared catalysts. The energy dispersive x- ray spectroscopy (EDX) analysis was used to confirm the chemical composition as well as homogeneous distribution of prepared catalysts calcined at 500^{0}C were depicted in the Figure.3(a), The EDX analysis data showed presence of Fe and Mo, Si and O elements in the synthesized catalysts. Therefore the EDX confirmed the formation of various wt. % Fe/Mo/SiO_2 catalysts.

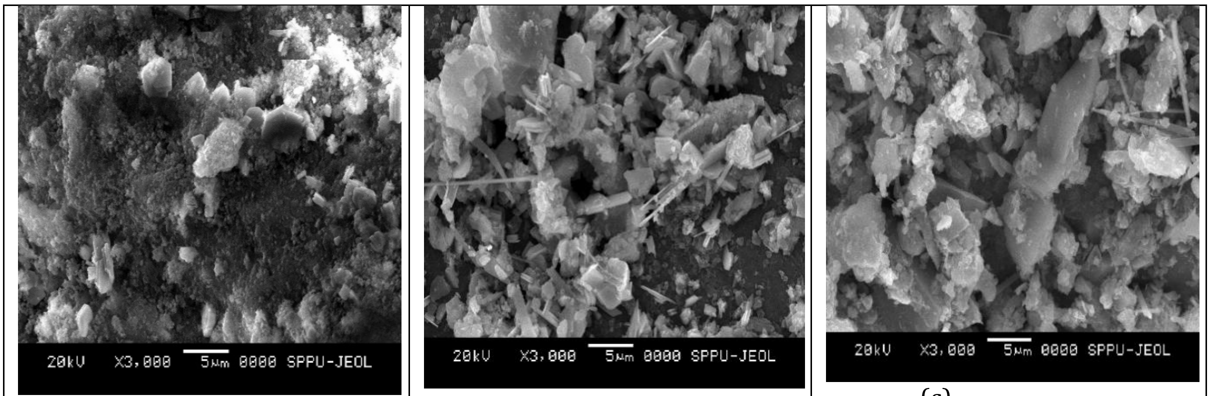

(a) (b) (c)

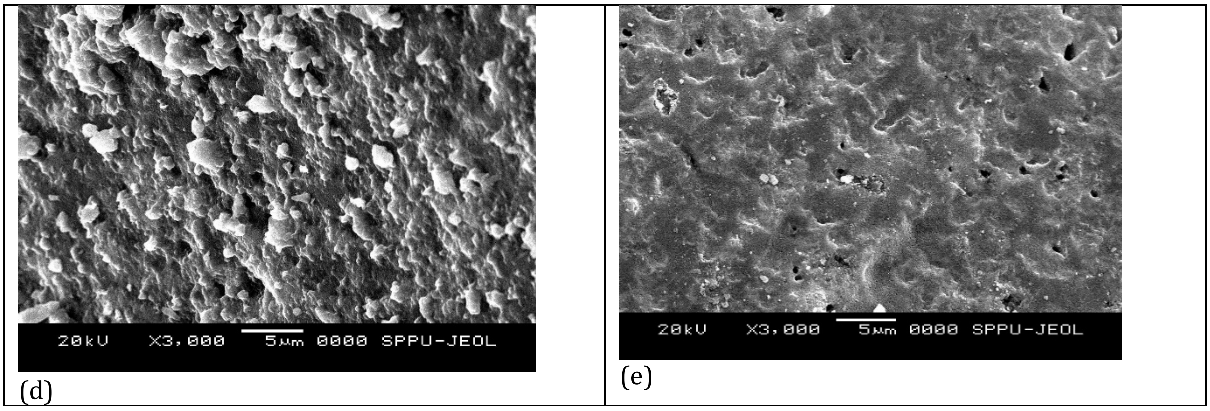

Figure.3(a)SEM graph of (a)1wt%, (b) 5wt%,(c) 10wt%,(d) 15wt% and (e) 20wt% Fe/MS

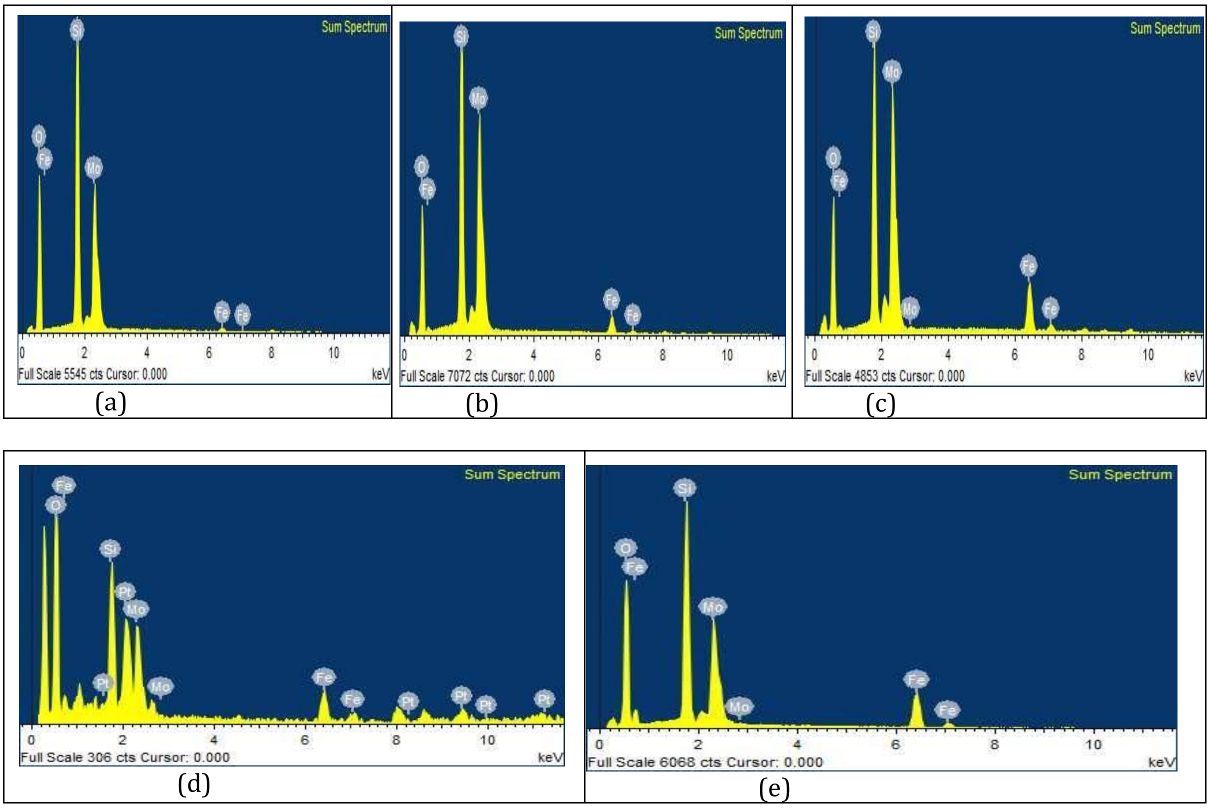

Figure.3(b) EDX graph of (a)1wt%, (b) 5wt%,(c) 10wt%,(d) 15wt% and (e) 20wt% Fe/MS

Ultra Violet Spectroscopy (UV):

UV absorption spectral study helped in understanding the electronic structure of the optical band gap of the material. Figure 4 (a) illustrates the UV-visible absorbance spectrum of synthesized Fe/MS (1-20wt%), which was measured in diffuse reflectance mode between 200 and 400 nm. The UV-visible absorbance spectrum showed band edge around 255 nm Strong absorption band in the UV-light region is clearly noticed and corresponding band gap observed to be 4.45 eV for 1wt% Fe/MS which is gradually decreased as concentration of material increased i.e 4.18eV for 20wt% which is clearly seen in figure 4(b)

The synthesized nanomaterial for optical measurements, absorption spectra can best represent explanation for light absorbed by that material. The absorbance spectrum of $Fe/Mo/SiO_2$ are illustrated in Fig. 4(a). The results showed a good absorbance towards visible region by the red shift to higher wavelengths occurred from 200 to 300 nm for Fe/Mo/SiO2, which assigned to photo excitation between the energy levels. From the absorption spectra, the exact band gap for these materials obtained from the delocalization of orbitals and also easy to recognize the matching between the materials. The results confirmed that the obtained band gap energy calculated from the absorption and bandgap for silica was 5 eV, which reduced to 4.18 eV by addition of Fe/Mo to silica to form Fe/MS nanocomposite. After knowing the energy of the materials, one can gain more insight about material whether it was cantered more to UV region and how the materials connect easily together.

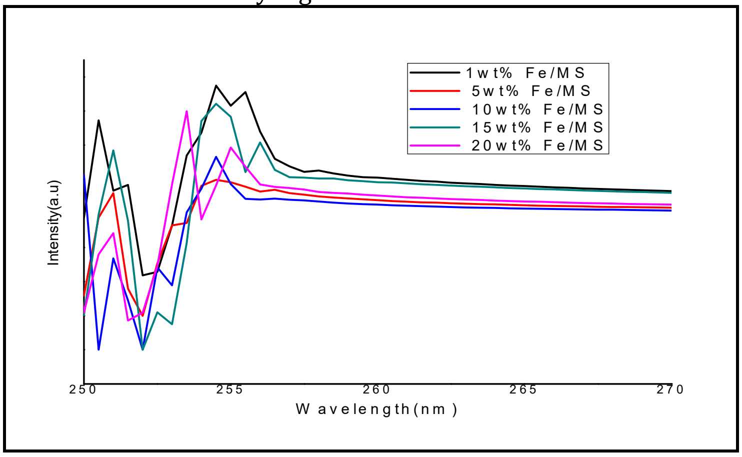

Figure 4(a) UV spectra of 1-20wt% FMS

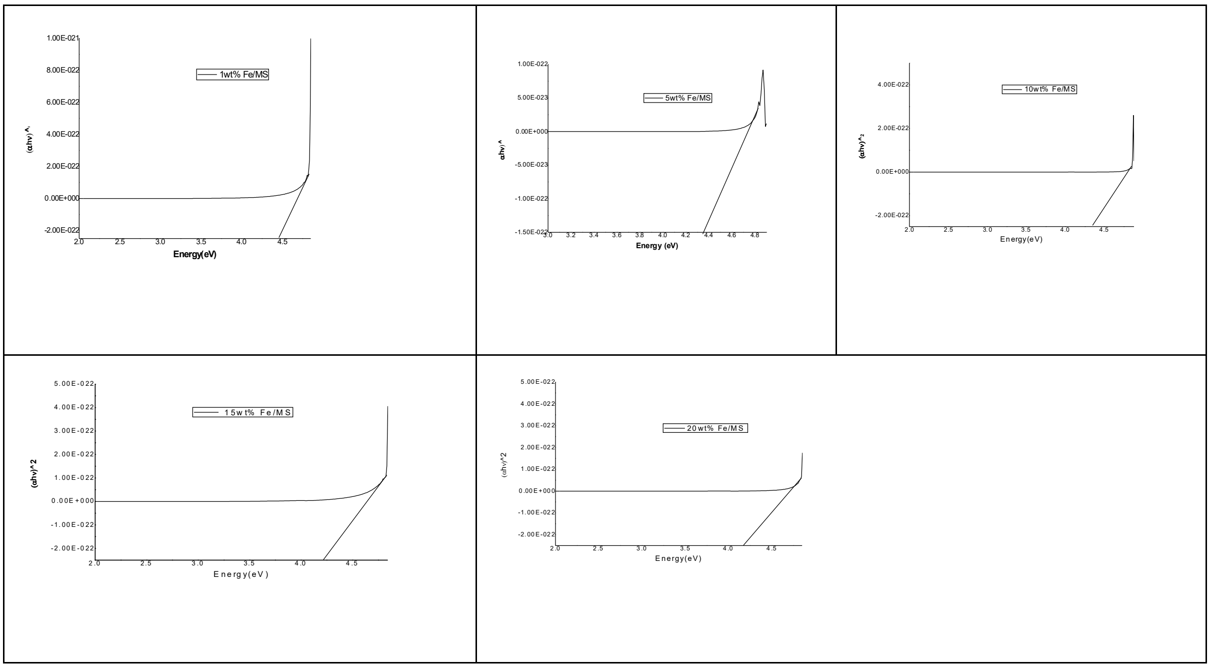

Figure 4 (b) Band Gap spectra for 1-20wt% FMS

f) Photocatalytic degradation:

For the photocatalytic applications of Fe doped Mo/Silica nanomaterials, four different kind synthetic dyes are selected. The phtocatalytic performance of acidic dyes like Methyl orange, Methyl red, Congo red and basic dyes such as Methylene blue in the presence of catalyst at different time intervals was observed. The photodegradation efficiency of the nanocatalyst has been determined.

Reaction Mechanism:

The general photocatalysis process and the involved photochemical reactions which are reported by literature is given following [26]

$$\text{FMS} + \text{Light energy } (h\upsilon) \rightarrow \text{FMS} + e^- + h^+$$

$$h^+ + H_2O \rightarrow H^+ + OH\bullet$$
$$h^+ + OH^- \rightarrow OH\bullet$$
$$e^- + O_2 \rightarrow O_2^-$$
$$2e^- + O_2 + 2H \rightarrow H_2O_2$$
$$\text{And } e^- + H_2O_2 \rightarrow OH\bullet + OH^-$$

Generally, the photocatalytic degradation involves several steps such as adsorption desorption, electron-hole pair production, recombination of electron pair and chemical reaction. The general mechanism of photodegradation of organic molecules is explained as follows. When the nanocatalyst is irradiated with photons of energy equal to or more than band gap energy of nanocatalyst, the electrons (e−) are excited from the valence band (VB) to the conduction band (CB) with the simultaneous creation of holes (h+) in the valence band. If the positively charged holes and negatively charged electrons required longer to combine again, the catalyst could operate more effectively. H+ and OH• are produced when the catalyst is in aqueous solution and exposed to light. In order to further promote the OH- ion and OH• free radical, the photogenerated electrons subsequently interact with trapped O_2 and H+ to produce H_2O_2. As a result, highly reactive radical species were produced, allowing them an additional opportunity to interact with the pollutant dyes OH• and inhibit the recombination of holes and electrons, which are charge carriers.[14]. The photocatalytic activities of the Fe/Mo/SiO_2 nanocatalysts have been investigated by different dye degradation under visible light and photo degradation efficiency has been determined as follow:
Degradation Efficiency = Ao – At/Ao ×100
Where A0 and At are the absorbance quantity of Dye solution at zero minute and a time 't' respectively.
The photo catalytic degradation results of Fe doped Mo/SiO_2 nanomaterials are presented in Fig. 5. As can be seen in Fig. 5, the degradation efficiencies for Methyl orange dye are 75, 78 and 82, 85 and 88 % for 1%, 5% ,10% 15% and 20% Fe/Mo/SiO_2 nanomaterials respectively.

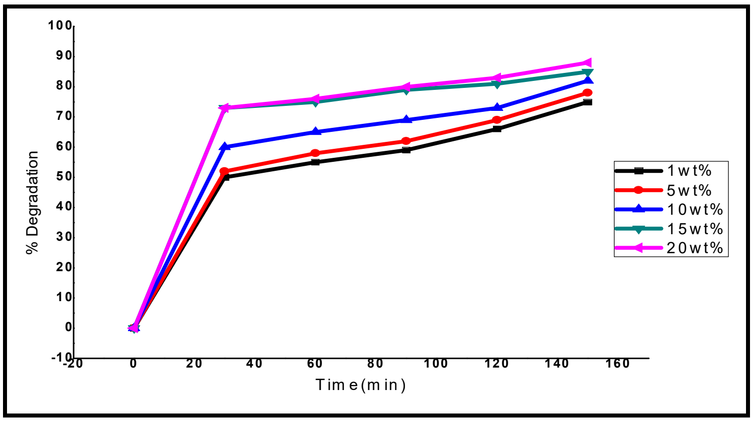

Figure 5.Methyl Orange % degradation spectra for 1-20wt% FMS

These results clearly showed that 20% of Fe doped Mo/SiO_2 was optimum concentration which has depleted concentration of dye by 88% within 150 min. It means 20% of Fe doped Mo/SiO_2 showed highest photocatalytic activity.

Antimicrobial Activity of FMS NPs

Earlier Literature reported that nanoparticles of iron oxide inhibit the bacterial activity. Fe(III) played very important role in biomedicine because of its superparamagnetic nature, therefore used in diagnosis and treatment (Prucek et al 2011, Gordon et al 2011, Azam et al 2012). These nanoparticles coating may allow few antimicrobial agents to go inside the body due to its magnetic nature. Hence this bacterial activity of iron oxide is very important for medicine point of view. Therefore, it is very essential to study for enhancement of activity of iron oxide for medicine and diagnosis purpose. In this work, we studied the antibacterial test on Gram +Ve , Gram –Ve and Fungal species. Antibacterial sensitivity test was carried out by well diffusion method and results are presented in below table 1a and 1b. It was observed that after keeping for longer period the inhibition zones were increased. Here Inhibition zones were examined after incubation period. Recorded zone of inhibition in mm and showed in table 1a and 1b. These results were confirmed the activity of the synthesized nanomaterial. The antibacterial activity results of 1wt % Fe/Mo/SiO_2 showed moderate antimicrobial activity whereas 20wt % Fe/Mo/SiO_2 showed better antimicrobial activity against pathogenic bacterium and fungal species. There are many factors responsible for the antibacterial activity of iron doped oxide nanoparticles. The main mechanism by which these particles showed antibacterial activity might be b 107 via oxidative stress generated by Reactive Oxygen Species (ROS). ROS, including superoxide radicals (O_2–), hydroxyl radicals (–OH), hydrogen peroxide (H_2O_2) and singlet oxygen (1 O_2), can cause damage to proteins in bacteria. In this study, Iron oxide could be the source that created ROS leading to the inhibition of the pathogenic bacteria. The antibacterial activity of FMS nanomaterials results revealed as an excellent antibacterial agent against gram positive and gram negative bacteria. Further, it has been confirmed that the concentration of 20 wt% FMS NPs exhibited large zone of inhibition on bacterial growth than concentration of 1% FMS NPs. It appears that the antibacterial activity of the nanomaterials increased with increase in concentrations of iron oxide nanoparticles.

Table.1(a). Zone of inhibition in mm for Fe/MS materials for microbial strains.

	Zone of inhibition in mm			
Catalyst %	***S. aureus***	***B. subtilis***	***E.coli***	***K.pneumoniae***
1wt% Fe/MS	32 ± 0.01	20 ± 0.02	15 ± 0.02	21 ± 0.02
5wt% Fe/MS	24 ± 0.01	22 ± 0.01	19 ± 0.01	22 ± 0.03
10wt% Fe/MS	35 ± 0.03	26 ± 0.02	21 ± 0.02	20 ± 0.01
15wt% Fe/MS	32 ± 0.02	28 ± 0.02	22 ± 0.01	24 ± 0.02
20wt% Fe/MS	36 ± 0.01	27 ± 0.01	24 ± 0.03	22 ± 0.03
Std. Streptomycin	26 ± 0.04	17 ± 0.03	17 ± 0.02	19 ± 0.03
Control (DMSO)	00	00	00	00

Table.1(b). Zone of inhibition in mm for Fe/MS materials for Fungal strains.

Catalyst %	***Candida albicans***	***Aspergillus niger***
1wt% Fe/MS	21 ± 0.02	05 ± 0.01
5wt% Fe/MS	24 ± 0.03	10 ± 0.03
10wt% Fe/MS	27 ± 0.03	09 ± 0.03
15wt% Fe/MS	29 ± 0.01	08 ± 0.02
20wt% Fe/MS	32 ± 0.02	10 ± 0.01
Std. flucanozole	22 ± 0.02	01 ± 0.03
Control (DMSO)	00	00

Antibiofilm activity:

Table 2(a) Antibiofilm activity for *Staphylococcus aureus*:-

Nanoparticles / Concentration	**FMS (Absorbance)**
1%	0.160
5%	0.171
10%	0.148
15%	0.130
20%	0.124

Negative control – 0.094
Positive control – 0.198

Table 2(b) Antibiofilm activity for *Pseudomonas aeruginosa*:-

Negative control – 0.094

Nanoparticles / Concentration	**FMS (Absorbance)**
1%	0.170
5%	0.186
10%	0.150
15%	0.148
20%	0.140

Positive control – 0.252

Table 2(c) Antibiofilm activity for *E. coli*:-

Nanoparticles / Concentration	FMS (Absorbance)
1%	0.196
5%	0.193
10%	0.189
15%	0.164
20%	0.141

Negative control – 0.094
Positive control – 0.229

The formulated Fe supported on MoO_3/SiO_2 (FMS) catalyst was subjected to the set of experiments against the 3-test organism to determine its anti-biofilm activity. The results of biofilm formation inhibition as per Table 1(a, b, c).

CONCLUSION

The nanocrystalline iron oxide doped Mo/SiO_2 were synthesized by sol-gel method with an average diameter of 40 nm. This environment friendly method of synthesizing FMS nanomaterial and its application as an antibacterial agent and its Photo degradation against industrial dyes also explored and showed its application in effluents treatment in various industries. It also opens the doors for further research in the medicine and diagnosis fields for its use in human being. In this section it has been concluded that FMS NPs showed better antibacterial activity as well as photo catalytic activity. From the antibacterial and antifungal study, it is concluded that 20% Fe/MS nano catalyst show the highest zone of inhibition for both microbial as well as fungal species and suitable for antibiotic applications. For antibiofilm activity, it is concluded that the FMS catalysts significantly reduce biofilm formation of *Staphylococcus aureus*, *Pseudomonas aeruginosa* and *E. coli* as the concentration of FMS increases. The result indicated that photo catalytic activity, antimicrobial and antibiofilm activity is increased with increase in concentration of catalysts.

Conflict of Interest: Authors declare that there is no conflict of interest.

REFERENCES

1. M. M. Hasan, M. A. Shenashen, M. N. Hasan, H. Znad, M. S. Salman and M. R. Awual (2021) Natural biodegradable polymeric bioadsorbents for efficient cationic dye encapsulation from wastewater, J. Mol. Liq., 323, 114587, DOI: 10.1016/j.molliq.2020.114587.
2. Bruno Lellis Díntia, Zani Fávaro-PolonioJoão Alencar Pamphile, (2019) Biotechnology Research and Innovation , 3(2), 275-290.
3. M. Isik and D. T. Sponza, (2005) Bioresour. Technol. 96, 633.
4. Bhat IU, Anwar MNK, Appaturi JN. (2019) Polymer based palladium nanocatalyst for the degradation of nitrate and Congo red. J Polym Environ; 27: 1475-87. http://dx.doi.org/10.1007/s10924-019-01444-9
5. Khan MMR, Akter M, Amin MK, Younus M, Chakraborty N. (2018) Synthesis, luminescence and thermal properties of PVA-$ZnOAl_2O_3$ composite films: towards fabrication of sunlight-induced catalyst for organic dye removal. J Polym Environ; 26: 3371- 81.
6. R. N. Bharagava, G. Saxena and S. I. Mulla, (2020) Introduction to Industrial Wastes Containing Organic and Inorganic Pollutants and Bioremediation Approaches for Environmental Management, in Bioremediation of Industrial Waste for Environmental Safety, Springer Singapore,. 1–18, DOI: 10.1007/978-981-13-1891-7_1.
7. Muhammad Ismail, Kalsoom Akhtar, M.I. Khan, Tahseen Kamal, Murad Ali Khan, Abdullah M. Asiri, Jongchul Seo and Sher Bahadar Khan, (2019) Pollution, Toxicity and Carcinogenicity of Organic Dyes and their Catalytic Bio-Remediation, Current Pharmaceutical Design, 25, 3653-3671.
8. F. Raposo, M. A. De La Rubia and R. Borja, (2009) Methylene blue number as useful indicator to evaluate the adsorptive capacity of granular activated carbon in batch mode: in�uence of adsorbate/adsorbent mass ratio and particle size, J. Hazard. Mater., 165, 291–299, DOI: 10.1016/ j.jhazmat.2008.09.106.
9. Z. Yuan, J. Wang, Y. Wang, Q. Liu, Y. Zhong, Y. Wang, L. Li, S. F. Lincoln and X. Guo, (2019) Preparation of a poly(acrylic acid) based hydrogel with fast adsorption rate and high adsorption capacity for the removal of cationic dyes, RSC Adv., 9, 21075–21085, DOI: 10.1039/c9ra03077h.
10. Englande AJ Jr, Krenkel P, Shamas J. (2015) Wastewater Treatment &Water Reclamation. Reference Module in Earth Systems and Environmental Sciences.:B978-0-12-409548-9.09508-7. doi: 10.1016/B978-0-12-409548-9.09508-7. Epub 22. PMCID: PMC7158167.
11. H. Wu, J. Dai, S. Sun, C. Du, Y. Long, H. Chen, G. Yu, S. Ye and J. Chen, (2021) Responses of habitat suitability for migratory birds to increased water level during middle of dry season in the two largest freshwater lake wetlands of China, Ecol. Indic., 121, 107065, DOI: 10.1016/ j.ecolind.2020.107065.

12. J. Fito, N. Tefera and S. W. H. Van Hulle, (2019) An Integrated Treatment Technology for Blended Wastewater of the Sugar Industry and Ethanol Distillery, Environ. Processes, 6, 475–491, DOI: 10.1007/s40710-019-00366-x.
13. S. Ye, W. Xiong, J. Liang, H. Yang, H. Wu, C. Zhou, L. Du, J. Guo, W. Wang, L. Xiang, G. Zeng and X. Tan, (2021) Re□ned regulation and nitrogen doping of biochar derived from ramie □ber by deep eutectic solvents (DESs) for catalytic persulfate activation toward non-radical organics degradation and disinfection, *J. Colloid Interface Sci.,* 601, 544–555, DOI: 10.1016/j.jcis.2021.05.080.
14. Audrey Moores, Ning Yan, (2017) Novel Catalytic Materials for Energy and the Environment *ACS Sustainable Chemistry & Engineering*, *5* (12), 11124-11124 DOI: 10.1021/acssuschemeng.7b04217
15. Ezzat Alnakip, Mohamed et al.(2014) "The Immunology of Mammary Gland of Dairy Ruminants between Healthy and Inflammatory Conditions." *Journal of veterinary medicine* vol. 2014 (2014): 659801. doi:10.1155/2014/659801
16. Aslam, Bilal et al.(2018) Antibiotic resistance: a rundown of a global crisis. *Infection and drug resistance* vol. 11 1645-1658., doi:10.2147/IDR.S173867.
17. Murthy S. Chavali, Maria P. Nikolova, (2019) Metal oxide nanoparticles and their applications in nanotechnology, SN Applied Sciences 1:607.
18. S. A. Ansari, M. M. Khan, M. O. Ansari, J. Lee and M. H. Cho, (2013) Biogenic synthesis, photocatalytic, and photoelectrochemical performance of Ag–ZnO nanocomposite, J. Phys. Chem. C, 117, 27023–27030, DOI: 10.1021/jp410063p.
19. C Siriwong,N Wetchakun, Burapat Inceesungvorn, Duangdao Channei, T Samerjai, Sukon Phanichphant, (2012) Doped-metal oxide nanoparticles for use as photocatalysts, Progress in Crystal Growth and Characterization of Materials 58(2-3):145-163
20. F. Yi, H. Gan, H. Jin, W. Zhao, K. Zhang, H. Jin, H. Zhang, Y. Qian and J. Ma, (2020) Sulfur- and chlorine-co-doped g-C3N4 nanosheets with enhanced active species generation for boosting visible-light photodegradation activity, Sep. Purif. Technol., 233, 115997, DOI: 10.1016/j.seppur.2019.115997.
21. F. Yi, J. Liu, G. Liang, X. Xiao and H. Wang, (2022) Insight into the enhanced degradation mechanism of g-C3N4/g-C3N5 heterostructures through photocatalytic molecular oxygen activation in Van der Waals junction and excitation, J. Alloys Compd., 905, 164064, DOI: 10.1016/ j.jallcom.2022.164064.
22. Abhijeet Mishra and Meryam Sardar (2014) Isolation of Genomic DNA by Silane-Modified Iron Oxide Nanoparticle, Enzyme Technology Lab, Department of Biosciences., 309-315.
23. Vinod B. Mane, Jayamala M. Deshmukh, Shobha A Waghmode and Sharda P. Dagade, (2015), Surface Characterization and Catalytic Activity of Cobalt Promoted MoO_3/SiO_2 Solid Acid Catalysts, Int.J. Chem. Tech Res.,8(8):310-317.
24. Raun Kristian Viegaard, Lundegaard Lars Fahl, Chevallier Jacques, Beato, (2018), Deactivation behavior of an iron-molybdate catalyst during selective oxidation of methanol to formaldehyde, Catal. Sci. Technol.,8:4626-4637.
25. Habibi M. H. and Karimi B. (2014), Preparation of nanostructure CuO/ZnO mixed oxide by sol–gel thermal decomposition of a CuCO3 and ZnCO3: TG, DTG, XRD, FESEM and DRS investigations, Journal of Industrial and Engineering Chemistry, 20(3): 925–929.
26. Mazaheri H., Ghaedi M., Azqhandi M.H.A. and Asfarama A., (2017) Application of machine/statistical learning, artificial intelligence and statistical experimental design for the modeling and optimization of methylene blue and Cd(II) removal from a binary aqueous solution by natural walnut carbon, Physical Chemistry Chemical Physics, 19, 11299- 11317.
27. Lemos JA, Abranches J, Koo H, Marquis RE, Burne RA. (2010). Protocols to study the physiology of oral biofilms. Methods Mol Biol.666:87-102. doi: 10.1007/978-1-60761-820-1_7
28. Mário Fernandes, Noelia González-Ballesteros, André da Costa, Raúl Machado, Andreia C. Gomes, Maria Carmen Rodríguez-Argüelles (2023). Antimicrobial and anti-bioflm activity of silver nanoparticles biosynthesized with Cystoseira algae extracts. JBIC Journal of Biological Inorganic Chemistry (Springer). 28:439–450.

CITATION OF THIS ARTICLE

Prashant Shinde, Mukund Ambawade, Shobha Waghmode and Sharda Gadale. Investigation of Structural Characterization and Biological applications of supported MoO_3/SiO_2 nanocomposite. Bull. Env. Pharmacol. Life Sci., Vol 13 [7] June 2024: 115-124